Temperature dependence of Raman scattering in $K_3Ba_3C_{60}$

1999 J. Phys.: Condens. Matter 11 8329

(http://iopscience.iop.org/0953-8984/11/42/313)

J. Phys.: Condens. Matter **11** (1999) 8329–8340. Printed in the UK PII: S0953-8984(99)05632-5

Temperature dependence of Raman scattering in $K_3Ba_3C_{60}$

X H Chen†‡, Y M Xiong†, Z Sun†, T Takenobu‡, H Kitagawa‡ and Y Iwasa‡

† Structural Research Laboratory and Department of Physics, University of Science and Technology of China, Hefei, Anhui 230026, People's Republic of China
‡ Japan Advanced Institute of Science and Technology, Tatsunokuchi, Ishikawa 923-1292, Japan

Received 29 June 1999

Abstract. Raman spectra at different temperatures are reported for $K_3Ba_3C_{60}$. A systematic change of the Raman spectra with temperature is observed. The development of the linewidth and intensity for all modes with decreasing temperature is in sharp contrast to the case for pure C_{60}. For the two lowest-frequency H_g modes, the appearance of the low-frequency components and an increase in their intensity are observed as temperature decreases. This could be related to an internal strain between the doped part of the crystal and the undoped part of the crystal, and the Jahn–Teller effect. An anomalously large upshift of 9 cm^{-1} between 20 K and room temperature for the pinch $A_g(2)$ mode suggests the existence of hybridization between the C_{60} molecules and the intercalants. The doublet of $A_g(1)$ at low temperature could arise from the splitting of the crystal field.

1. Introduction

Raman spectroscopy has played an important role since the beginning of the research on C_{60}. The Raman band of the $A_g(2)$ intramolecular vibrational mode softens when alkali metal is doped into C_{60} crystals or films [1–3]. This feature has been used to estimate the concentration of the doped alkali metal. Raman scattering has been widely used to deduce the electron–phonon coupling constant λ for the superconducting fullerides on the basis of analysis of the linewidths [3–6]. The results reveal that the pairing is mediated by a phonon with a weak coupling in the superconducting state.

Modifications of C_{60} Raman spectra are expected in the phase transition from face-centred cubic (fcc) to simple cubic (sc) structure, in particular those connected with change of the crystal-field symmetry in fullerides. A great deal of Raman work was done on the changes that occur in low-temperature Raman spectra, including line splittings, and intensity and frequency shifts of intramolecular vibrations [7–10]. These features have been assigned to a ^{13}C isotope effect [11], sample disorder [12], and crystal-field effects [13]. Van Loosdrecht *et al* have reported that discontinuous changes in the frequencies and bandwidths of the intramolecular vibrational modes occur near the fcc–sc phase transition temperature, and the splitting and narrowing of the intramolecular modes. Several new modes have also been observed [7]. Recently, Winter and Kuzmany observed that the low-frequency $H_g(1)$ and $H_g(2)$ modes lose all degeneracy and split into five components, each of which couples differently to the t_{1u} electrons for single crystals of K_3C_{60} at 80 K [5].

A $K_3Ba_3C_{60}$ phase with a formal C_{60}^{9-} charge and half-filling of the t_{1g} band has recently been reported [14]. As the intercalation host, Ba_3C_{60} is a vacancy-ordered derivative of the bcc A_6C_{60} structure with half of the cation sites empty (A15 structure). Three alkali metal cations

0953-8984/99/428329+12$30.00

are introduced into Ba_3C_{60} to form a cation-disordered $K_3Ba_3C_{60}$ phase isostructural with A_6C_{60}. $K_3Ba_3C_{60}$ with a half-filled t_{1g} band exhibits superconductivity at 5.6 K. However, the insertion of large A^+ cations leads to a decrease in T_c, in contrast to the behaviour of the A_3C_{60} phases [15].

In this work, we have measured the Raman spectra of $K_3Ba_3C_{60}$ at different temperatures in order to observe the development of asymmetric shapes for low-frequency H_g modes that have been described with Fano line shapes [16]. A systematic change of the Raman modes is observed with decreasing temperature. The $A_g(2)$ mode stiffens with decreasing temperature, and an upshift of 9 cm^{-1} is observed between room temperature and 20 K. A doublet is observed for the $A_g(1)$ mode, and the relative intensity of the two components systematically changes as a function of temperature. The intensity of the low-frequency components increases with decreasing temperature for the low-frequency $H_g(1)$ and $H_g(2)$ modes.

2. Experimental procedure

Samples of Ba_3C_{60} was synthesized by reacting stoichiometric amounts of powders of Ba and C_{60}. A quartz tube with mixed powder inside was sealed under a high vacuum of about 2×10^{-6} Torr, and heated at 550–600 °C for three days. Synthesis of $K_3Ba_3C_{60}$ was carried out in a similar manner to that for alkali doping into pure C_{60}. A piece of alkali and Ba_3C_{60} powder were loaded into a Pyrex tube, which was sealed under 2×10^{-6} Torr and calcined at 250 °C for three days. X-ray diffraction analysis was performed using a 4.5 kW rotating molybdenum anode as the x-ray generator and an imaging plate (IP, MAC, Science, DIP320V) as the detector. X-ray diffraction showed that all samples were single phase, which is also confirmed by the single peak feature of the pentagonal pinch $A_g(2)$ mode in the Raman spectra.

Raman scattering experiments were carried out using the 632.8 nm line of a He–Ne laser in the Brewster angle backscattering geometry. The scattering light was detected with a Dilor XY multichannel spectrometer using a spectral resolution of 3 cm^{-1}. In order to obtain good Raman spectra, the samples were ground and pressed into pellets with a pressure of about 20 kg cm^{-2}. The samples were mounted on the cold finger of a closed cryostat using silver paint. Cooling was achieved with liquid He flow. Measurements were performed in the temperature range from 2 K to room temperature in a vacuum at approximately 10^{-6} Torr.

3. Results and discussion

Figure 1 shows the Raman spectra at different temperatures for the polycrystalline sample of $K_3Ba_3C_{60}$. Only one peak of the pentagonal pinch $A_g(2)$ mode is observed, providing evidence that the sample is single phase. This agrees fairly well with the x-ray diffraction patterns. With decreasing temperature, the frequency of the pentagonal pinch $A_g(2)$ mode monotonically increases. There is an upshift of about 9 cm^{-1} between 295 K and 20 K for the frequency of the $A_g(2)$ mode, while only 3 cm^{-1} upshift is observed for the $A_g(1)$ mode. The positions (σ) and halfwidths (γ) of the Raman modes observed are listed in table 1. From figure 1, it can be seen that the high-frequency modes do not change with decreasing temperature except for a slight upshift of their frequencies. However, the low-frequency modes change very much—including the intensity and halfwidth—and some new modes are also observed in the low-frequency range. It is worthy of note that the intensity decreases and the halfwidth broadens for all modes with decreasing temperature. This is in contrast to the case for pure C_{60}, in which splitting and narrowing of the intramolecular modes and an increase in intensity are observed [7, 8]. However, the intensity of the low-frequency modes

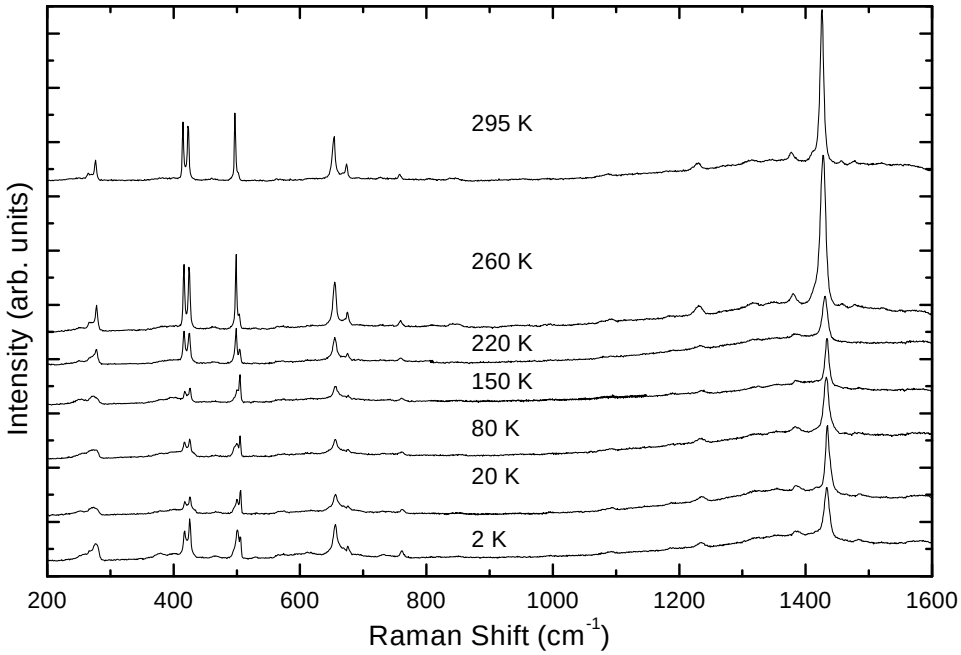

Figure 1. Raman spectra of $K_3Ba_3C_{60}$ at various temperatures.

increases at 2 K relative to that at 20 K. This could be related to the electronic state, since the sample transfers from the metallic to the superconducting state at 5.6 K. The Raman intensity of the asymmetric H_g modes at resonance turns out to be very sensitive to the band-structure changes due to the vibrational mixing of the electronic bands [10]. In the following, we give a detailed analysis of the low-frequency H_g modes, and then discuss the A_g modes.

Figure 2 shows the results of a line-shape analysis of the Raman spectra of the $H_g(1)$ modes at different temperatures. All modes were fitted to a Lorentzian line shape. The spectrum at 295 K can be fitted by four components. An apparent doublet located at about 276.4 and 266.4 cm^{-1} is observed at 295 K, and there exist two weak peaks in the frequency range 230–255 cm^{-1}. With decreasing temperature, the two high-frequency components are integrated into one broadening peak, so the fitting with one component is not good on the high-frequency side, while the intensity of the weak peaks on the low-frequency side apparently increases. A doublet with two broadening peaks is observed in the temperature range 150–20 K. At 2 K, the doublet is split into four components. A similar splitting has been observed for single-crystal K_3C_{60} at 80 K [5], in which the $H_g(1)$ mode is split into five components, and in Ba_4C_{60} and Ba_6C_{60} at room temperature [6].

Figure 3 shows the higher-resolution Raman spectra in the frequency range 320–450 cm^{-1} at different temperatures. Only a doublet of $H_g(2)$ is observed at 295 K. With decreasing temperature, the new components appear on the low-frequency side, and their intensities increase. The $H_g(2)$ mode is apparently split into four components below 150 K. The frequency of the four components is nearly the same as that observed for K_3C_{60} at 80 K. This splitting of the $H_g(2)$ mode in $K_3Ba_3C_{60}$ with bcc structure is unexpected, since the group theoretical consideration predicts a splitting into two in the space group $I_{m\bar{3}}$ (T_5^h). Similar behaviour has

Table 1. Positions and linewidths (in parentheses) for the Raman modes in $K_3Ba_3C_{60}$ at different temperatures.

I_h mode	2 K $\omega(\gamma)$ (cm^{-1})	20 K $\omega(\gamma)$ (cm^{-1})	80 K $\omega(\gamma)$ (cm^{-1})	150 K $\omega(\gamma)$ (cm^{-1})	220 K $\omega(\gamma)$ (cm^{-1})	260 K $\omega(\gamma)$ (cm^{-1})	295 K $\omega(\gamma)$ (cm^{-1})
$A_g(1)$	500.5(6.8)	500.1(7.5)	499.8(11.1)	500.2(5.0)	498.8(3.6)	498.8(2.7)	497.3(2.4)
	505.6(2.8)	505.7(1.3)	505.4(2.3)	504.8(1.6)	504.7(1.9)	504.0(2.1)	502.4(2.1)
$A_g(2)$	1433.4(9.2)	1434.5(7.6)	1432.7(9.1)	1433.0(7.3)	1430.5(9.1)	1427.4(9.2)	1425.7(6.6)
$H_g(1)$	234.8(17.1)						235.6(15.0)
	255.8(14.4)	251.3(24.8)	255.5(29.8)	251.9(20.6)	249.6(15.2)	250.8(27.9)	249.4(10.3)
	268.9(10.8)				271.1(14.3)	269.1(9.8)	266.4(9.8)
	277.3(6.9)	273.1(13.5)	273.5(16.8)	273.3(12.6)	277.8(3.7)	278.1(3.7)	276.4(3.3)
$H_g(2)$	378.8(16.0)	377.4(17.6)	377.8(20.7)	378.2(20.7)	382.8(23.6)	380.6(12.3)	
	399.7(22.9)	400.8(21.8)	401.1(30.2)	399.5(23.8)	399.8(17.2)	399.9(10.2)	
	417.7(5.0)	418.1(5.6)	417.3(4.7)	418.3(4.9)	416.3(3.6)	416.5(2.8)	414.9(2.3)
	425.4(4.2)	425.9(5.1)	425.3(4.1)	425.7(3.8)	424.6(4.3)	424.4(2.1)	422.9(2.8)
$H_g(3)$	655.9(8.8)	656.1(10.4)	655.7(10.0)	655.9(9.8)	655.0(8.0)	654.8(6.0)	653.5(5.4)
	675.5(6.9)	673.2(18.1)	674.8(12.0)	673.4(34.6)	674.8(6.9)	674.7(6.4)	673.3(4.6)
$H_g(4)$	761(4.2)	761.9(7.3)	760.7(8.5)	760.0(6.2)	758.2(6.9)	759.1(4.7)	757.7(3.7)
$H_g(5)$	1090.4(6.8)	1093.1(9.8)	1090.0(19.3)	1090.1(13.2)	1089.8(14.6)	1092.4(21.9)	1086.2(13.3)
$H_g(6)$	1187.6(15.8)	1189.2(13.0)	1188.5(16.4)	1190.7(15.5)	1189.8(9.0)	1185.6(17.8)	1184.1(15.4)
	1233.8(14.4)	1234.9(15.1)	1233.0(12.6)	1235.0(11.1)	1232.2(10.8)	1230.6(13.6)	1229.0(12.2)
$H_g(7)$	1318.8(19.8)	1319.3(20.9)	1316.8(8.2)	1322.8(16.6)	1317.8(18.1)	1316.3(9.4)	1314.6(19.9)
	1385.3(11.9)	1387.6(13.0)	1384.1(15.6)	1384.1(3.7)	1384.9(11.8)	1380.5(9.6)	1377.3(8.0)
$H_g(8)$	1484.7(8.8)	1486.2(8.1)	1483.4(16.6)	1484.1(6.0)		1478.8(12.2)	1476.9(7.7)

also been observed for Ba_6C_{60} with bcc structure at room temperature [6].

For the degeneracy lifting of low-frequency H_g modes in K_3C_{60} single crystal at 80 K, Winter and Kuzmany gave several possible explanations.

(1) The splitting of the mode is understood on the basis of the merohedral disorder for the alkali-derived metallic fullerides [17]. This disorder is of sufficiently low symmetry to allow only one-dimensional representations for all modes.
(2) The splitting originates from a Jahn–Teller-type interaction. This interaction can give rise to a new vibrational system with a rather large number of components—possibly even more than five [18].

Also, a contribution to the splitting could come from an internal strain between the doped part of the crystal and the undoped part of the crystal. In our experiments, the low-frequency H_g modes lose almost all degeneracy at low temperature. It is found that the intensity of the new components continuously increases with decreasing temperature. This is different from the case for pure C_{60}, in which the most noticeable effect was a large increase in scattering intensity of the C_{60} Raman-active modes with decreasing temperature, especially in the range below the phase transition [10]. The temperature effect on the intensity and linewidth is in sharp contrast to that in the case for pure C_{60}. In short, a continuous temperature effect on the intensity and linewidth for new components of low-frequency H_g modes is observed. This would be expected if the internal strain between the doped part of the crystal and the undoped part of the crystal were responsible for the splitting of the low-frequency H_g modes. In this paper, by the doped and undoped parts of the crystal we mean the doped-cation-occupied

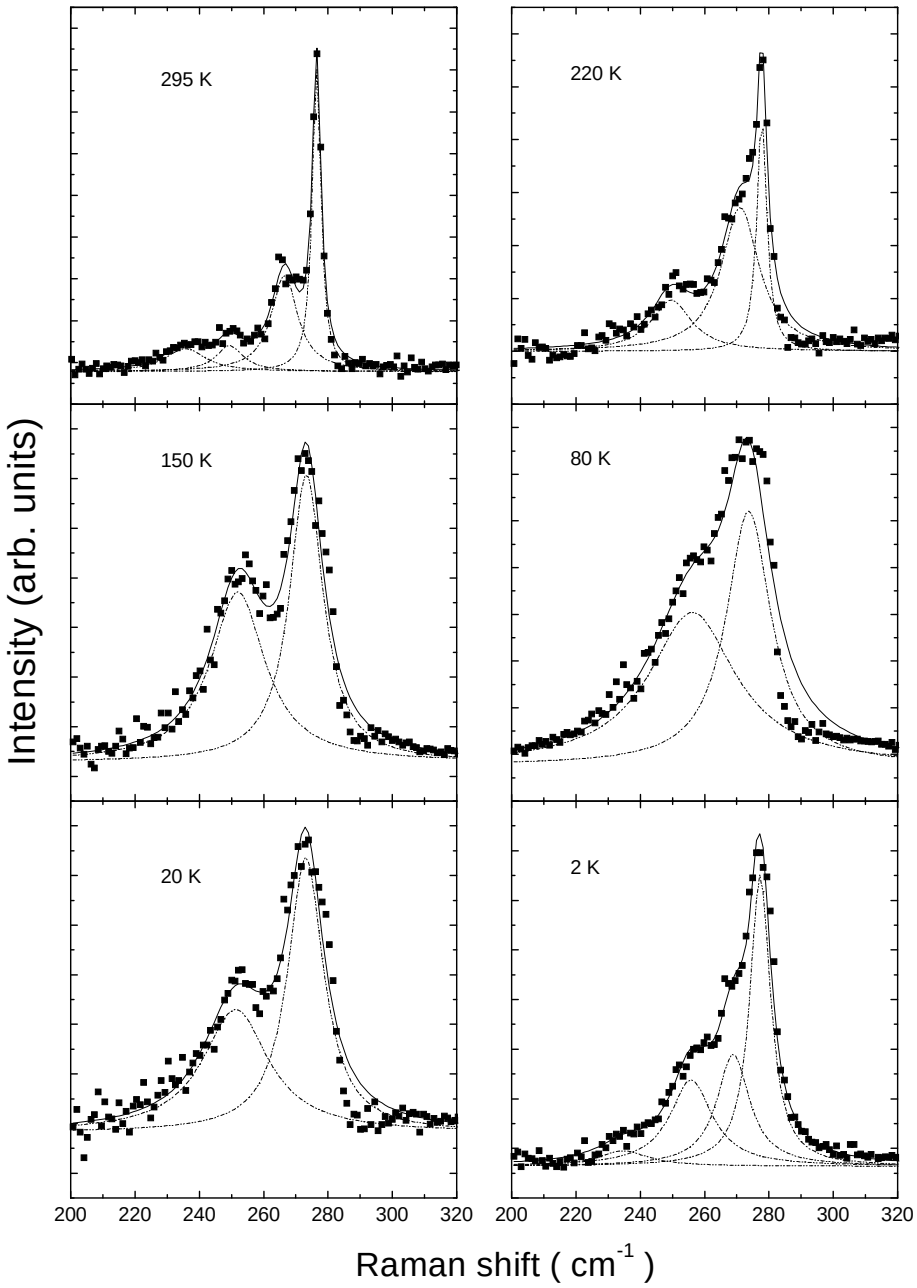

Figure 2. Raman spectra of the $H_g(1)$ mode at various temperatures for $K_3Ba_3C_{60}$. The dashed lines are computer fits for the individual components, which add up to the full line superimposed on the experimental results in each panel.

region and the region unoccupied by intercalants in the unit cell. In the case of $K_3Ba_3C_{60}$, alternative explanations for the splitting cannot be excluded on the basis of the Jahn–Teller-type interaction.

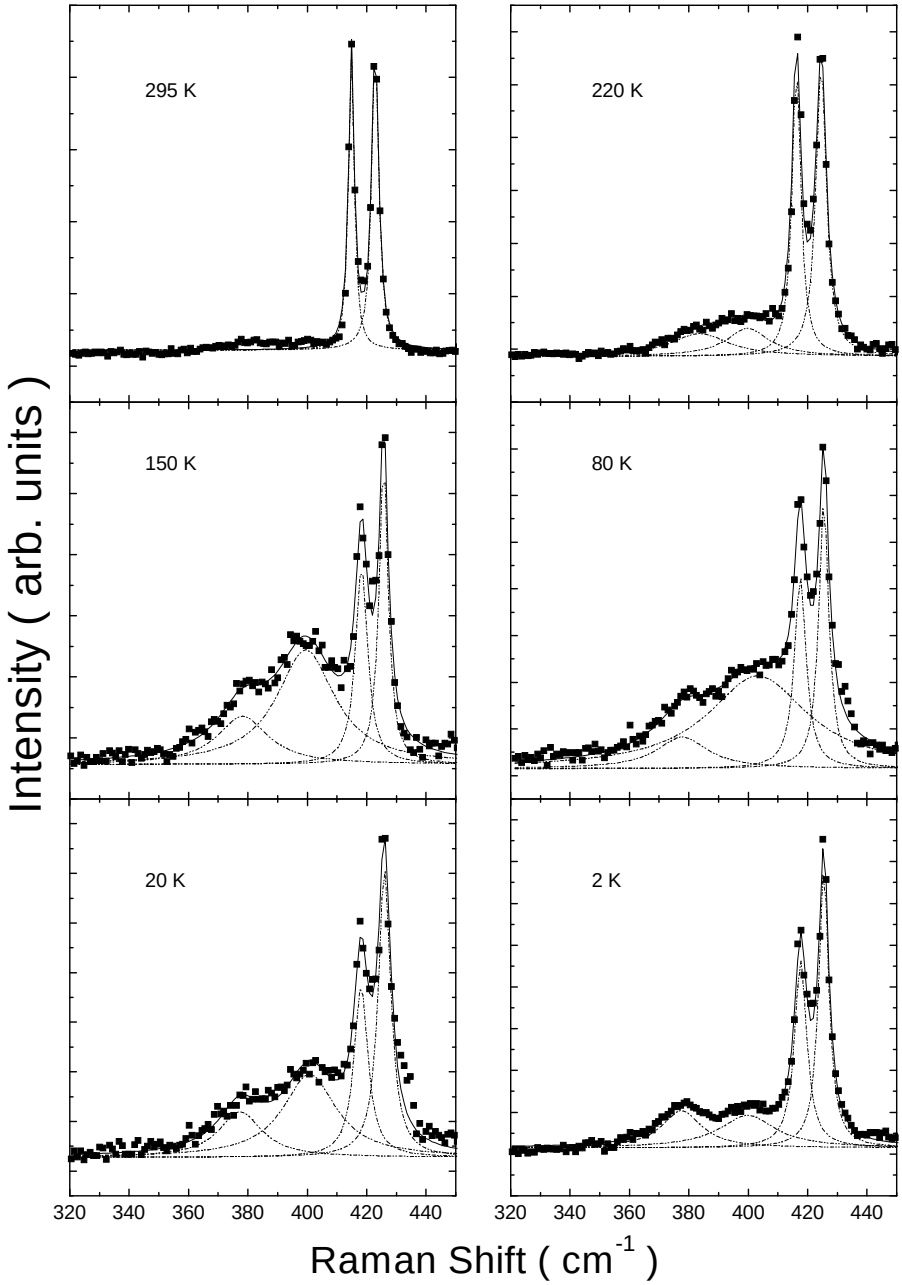

Figure 3. Raman spectra of the $H_g(2)$ mode at various temperatures for $K_3Ba_3C_{60}$. The dashed lines and full lines have the same meanings as in figure 2.

Figure 4 shows the Raman spectra in the region of the radial A_g mode at different temperatures. At 295 K, a sharp peak located at about 497.3 cm^{-1} is observed; a weak peak appears on the high-frequency side. With decreasing temperature, the intensity of the

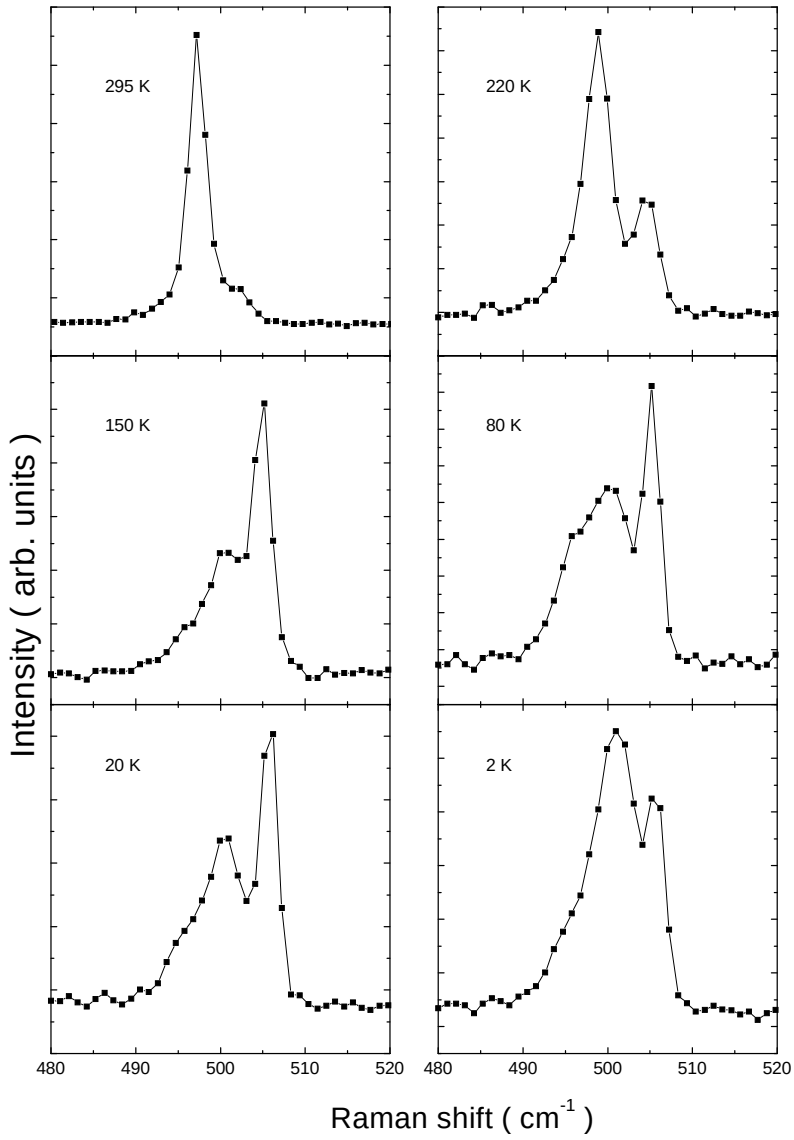

Figure 4. Raman spectra in the region of the radial A_g mode at different temperatures.

weak peak located at about 502.4 cm^{-1} continuously increases, while the intensity of the peak at 497.3 cm^{-1} decreases. At 150 K, the high-frequency peak becomes dominant. In the temperature range 20–150 K, the relative intensity of the two peaks remains nearly unchanged. As the temperature reduces to 2 K, the peak located on the low-frequency side becomes dominant again. This is consistent with the temperature dependence of the low-frequency H_g modes. It could be related to the electronic structure of the superconducting state. It has been observed that the two-A_g-mode line of pure C_{60} shows a splitting into two components at low temperature, which can be assigned to the $A_g + F_g$ representation in the low-temperature simple cubic structure [7, 8]. In fact, a very weak peak on the low-frequency side of the main band

for the $A_g(1)$ mode is also observed at room temperature for the C_{60} film. The intensity of the weak component increases with decreasing temperature [10]. This is consistent with what is observed for $K_3Ba_3C_{60}$. However, in the room temperature region, the single peak is observed at about 1468 cm^{-1} for single-crystal C_{60}. Two bands appear on the high-frequency side of the main band as the temperature is decreased. The two bands do not suddenly appear at one temperature; their intensities gradually increase [19]. The splitting of the A_g modes does not originate from the phase transition since the splitting takes place above the phase transition temperature and no phase transition is observed in the x-ray diffraction results for $K_3Ba_3C_{60}$. Crystal-field splitting could be responsible for the splitting of the $A_g(1)$ mode as mentioned above. Another cause for the splitting of the A_g modes could be an isotope effect [20].

Figure 5 shows the temperature dependence of the Raman shift for the two A_g modes. It shows that the frequency of the A_g modes increases as the temperature decreases. It is found that the frequency shift as a function of temperature is about 3 and 9 cm^{-1} between 20 K and room temperature for the $A_g(1)$ and $A_g(2)$ modes, respectively. These hardenings are consistent with the decrease of volume with decreasing temperature, resulting in an increase of force constant. The upshift of the A_g modes monotonically increases as temperature decreases. A similar behaviour has been reported for pure C_{60}, in which a frequency shift of 6 cm^{-1}, appearing rather abruptly at the first-order phase transition, is observed for the $A_g(2)$ mode [7,8]. Matus and Kuzmany pointed out [8] that this large shift of 6 cm^{-1} would be difficult to understand on the basis of (i) the reasonably well known response of pressure and temperature to the lattice constant [21,22] and (ii) the pressure coefficient for the frequency shift of the pinch mode [23]. The reported value for the latter is 4.9 cm^{-1} GPa^{-1}, which yields a total frequency shift of

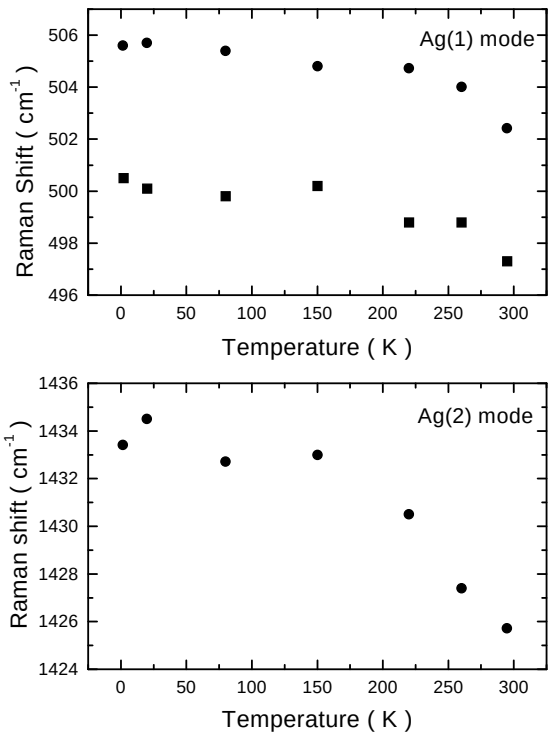

Figure 5. The temperature dependence of the Raman shift for the two A_g modes.

about 1 cm^{-1} for the whole frequency range between 0 K and room temperature. This suggests that this is indeed the range of frequency shifts that they observed for the internal modes of the fullerene molecule. However, some groups reported a small frequency shift of 1–2 cm^{-1} for the $A_g(2)$ mode between room temperature and 40 K, and no apparent increase of the frequency at the phase transition temperature [19, 24]. In the case of $K_3Ba_3C_{60}$, there is one conceivable cause for the upshift of the $A_g(2)$ mode other than the decrease of volume with decreasing temperature. It is well known that there exists a hybridization between alkaline-earth-atom states and the C_{60} π-states in alkaline-earth-metal-doped C_{60}. Raman scattering has indicated a similar hybridization in $K_3Ba_3C_{60}$ samples [25]. The hybridization becomes stronger as temperature decreases, resulting in a decrease in charge transfer, so the upshift of the $A_g(2)$ mode as a function of temperature is larger than that in pure C_{60} and alkali-metal-doped C_{60}, in which the hybridization is absent. It has been reported that the internal molecular modes show only slight change with temperature, and both A_g modes show a slight hardening of 1–2 cm^{-1} between 300 and 20 K in alkali-metal-doped C_{60} [4, 9]. This further supports the suggestion of an effect of hybridization on the frequency shift of $A_g(2)$ with decreasing temperature. It is worth pointing out that both A_g modes show a slight softening upon cooling below $T_c = 5.6$ K in our experiment, and a downshift of 1 cm^{-1} is observed for the $A_g(2)$ mode between 20 and 2 K. Similar behaviour is also observed for Rb_3C_{60} [9]. This suggests that the behaviour may be related to a superconducting transition.

Our experimental results show a sharp contrast to the case for pure C_{60} except for the appearance of several new lines. In the case of pure C_{60}, splitting and narrowing of the intramolecular modes are observed with decreasing temperature. In particular, the Raman scattering intensity of C_{60} intramolecular modes strongly increases upon cooling below room temperature. The relatively strong increase of the Raman intensity of the radial modes in the sc phase is attributed to their more effective modulation of the Coulomb interaction between oriented neighbouring C_{60} molecules [10]. In contrast, the intensity of the low-frequency modes continuously decreases and the intramolecular modes slightly broaden with decreasing temperature in $K_3Ba_3C_{60}$. This is different from the case for alkali-metal-doped C_{60}, in which the Raman spectrum exhibits very little temperature dependence between 300 and 15 K [4]. Why there exists a strong temperature dependence of the Raman spectrum for $K_3Ba_3C_{60}$ is not clear. It may be related to the hybridization between the C_{60} molecules and the intercalants.

The measurement of the phonon broadening provides rather direct information about the electron–phonon coupling. It is well known that the H_g modes are fivefold degenerate. Therefore, for the split modes a weighted average was used if not all of the five components could be determined explicitly. This is not a serious problem, since the narrow lines observed for the modes $H_g(3)$ to $H_g(6)$, where not all of the components could be determined, hardly contribute to the coupling [5]. However, the low-frequency $H_g(1)$ and $H_g(2)$ modes exhibit an asymmetric line shape characteristic of a Breit–Wigner–Fano resonance in fullerides [4]. This definitely leads to an error in determining the linewidth if the $H_g(1)$ and $H_g(2)$ modes do not completely split. Recently, the Raman spectrum for single crystals at low temperature was studied by Winter and Kuzmany. They found that the peaks for several of the H_g phonons were strongly asymmetric and could be fitted with five components for $H_g(1)$ and $H_g(2)$ modes [5]. This allows one to evaluate the electron–phonon coupling constants for all directly coupling components. The line shape obtained by Winter and Kuzmany raises questions about our understanding of how to analyse spectra. For $K_3Ba_3C_{60}$, the low-frequency $H_g(1)$ and $H_g(2)$ modes each split into four components at 2 K, while a doublet is observed for the $H_g(2)$ mode at 295 K. For comparison, the electron–phonon coupling constants are deduced on the basis of the Raman data at 2 K and 295 K, respectively. For the evaluation of the coupling constants as discussed below, a value of 5.6 eV^{-1} obtained from the normal-state susceptibility [15] is

used for the density of states $N(0)$.

The electron–phonon coupling constants are evaluated using Allen's formula

$$\gamma_i = \frac{1}{g_i}\frac{\pi}{2}N(0)\lambda_i\omega_{bi}^2 \tag{1}$$

where γ_i is the full width at half-maximum of the line, $N(0)$ is the density of states at the Fermi level per spin and molecule, and g_i and ω_{bi} are the mode degeneracy and the frequency before any coupling to the electrons has occurred, respectively. Allen's formula given above will be used to derive the coupling constants for the eight H_g modes. The frequency of the Raman modes for pure C_{60} is used as the bare phonon frequency. The averaged linewidths and the overall coupling constants for each mode and for all H_g modes at 2 and 295 K are listed in table 2, together with frequencies for the pure C_{60}. The averaged linewidths are directly evaluated from the linewidths in table 1. The values for λ_i are evaluated using equation (1).

Table 2. Positions, averaged linewidths, and electron–phonon coupling constants normalized to the density of states at the Fermi energy for eight fivefold-degenerate H_g modes at 295 K and 2 K.

		295 K		2 K	
Modes	ω (cm^{-1})	$\overline{\gamma}$ (cm^{-1})	$\lambda/N(E_F)$	$\overline{\gamma}$ (cm^{-1})	$\lambda/N(E_F)$
$H_g(1)$	270	10.1	0.110	12.3	0.137
$H_g(2)$	431	2.5	0.011	12.0	0.052
$H_g(3)$	709	5.0	0.007	7.8	0.012
$H_g(4)$	773	3.7	0.005	4.2	0.006
$H_g(5)$	1099	13.3	0.009	6.8	0.005
$H_g(6)$	1248	13.8	0.007	15.1	0.008
$H_g(7)$	1426	14.0	0.006	15.9	0.006
$H_g(8)$	1573	7.7	0.002	8.8	0.003
$\sum$			0.157		0.229

The individual contributions to the coupling constant from each H_g mode are listed in table 2. The two lowest-frequency H_g modes dominate the contribution to λ, yielding 78% and 83% of the total value at 295 K and 2 K, respectively. It should be noted that the averaged linewidth of the $H_g(2)$ mode at 2 K is much larger than that at 295 K, respectively. This arises from the appearance of the low-frequency components of the $H_g(2)$ mode at low temperature. These have large linewidths, leading to larger contributions to the coupling constant. This is consistent with what is observed for K_3C_{60} single crystal at 80 K [5]. The coupling constants obtained on the basis of the Raman data at 2 K and 295 K are nearly the same for the other modes. Therefore, one has to proceed with caution when analysing the low-frequency modes for the evaluation of the coupling constant. Within the BCS framework, the superconducting transition temperature T_c can be been deduced on the basis of the experimental values for λ by using the McMillan equation

$$T_c = \frac{\hbar\omega_{\ln}}{1.2k_B}\exp\left[\frac{-1.04(1+\lambda)}{\lambda-\mu^*-0.62\lambda\mu^*}\right]. \tag{2}$$

According to the observed frequencies and the coupling constants evaluated, the logarithmic averaged phonon frequency $\omega_{\ln}$ was determined as 380 and 377 cm^{-1} at 295 K and 2 K, respectively. With this value and λ, the superconducting transition temperature of 5.6 K can be evaluated, assuming the Coulomb repulsion between conduction electrons to have a μ^*-value of 0.28 at 295 K and 0.4 at 2 K, respectively—these are anomalously large. The value of μ^* is much larger than 0.18 for K_3C_{60} in the same way in the evaluation of T_c. Similar

behaviour has been observed for Ba_4C_{60} [6]. This might suggest a difference between t_{1u} and t_{1g} superconductors. To evaluate T_c, on the other hand, the logarithmic averaged phonon frequency of 150 K for the data for 295 K (62 K for the data for 2 K) is obtained if μ^* is set at a reasonable value of 0.2. This suggests that the phonon frequency is significantly smaller than the intramolecular vibration range. This is consistent with the result obtained from the normal-state susceptibility [15].

4. Conclusions

The Raman scattering of polycrystalline $K_3Ba_3C_{60}$ at different temperatures is studied. A systematic change of the Raman spectra with temperature is observed. In sharp contrast to the case for pure C_{60}, the intensities of the low-frequency modes decrease and the linewidths of all modes increase with decreasing temperature. The positions of all modes continuously shift to high frequency as temperature decreases. This arises from a decrease in volume and the increase of the force constant. An anomalously large upshift of 9 cm^{-1} for the pinch $A_g(2)$ mode suggests the existence of hybridization between the C_{60} molecules and the intercalants. A doublet of the $A_g(1)$ mode is observed at low temperature, and the relative intensity of the two components systematically changes as temperature decreases. For the two lowest-frequency H_g modes, an internal strain between the doped part of the crystal and the undoped part of the crystal, and the Jahn–Teller effect lead to the appearance of the low-frequency components and an increase in their intensity. The electron–phonon coupling constants are evaluated on the basis of the Raman data at 2 and 295 K, in the framework of Allen's theory. The results indicate that the contribution to the coupling constant from low-frequency modes is dominant. A change in intensity and linewidth is observed at the superconducting transition temperature.

Acknowledgments

This work was supported by a Grant from the Natural Science Foundation of China. The work in Japan was supported by the JSPS 'Future Programme' (RFTF96P00104), and also by a Grant-in-Aid for Scientific Research on the Priority Area 'Fullerenes and Nanotubes' from the Ministry of Education, Science, and Culture of Japan. X H Chen would like to thank the Inoue Foundation for Science for financial support.

References

[1] Duclos S J, Haddon R C, Glarum S, Hebard A F and Lyons K B 1991 *Science* **254** 1625
[2] Pichler T, Matus M, Küti J and Kuzmany H 1992 *Phys. Rev.* B **45** 13 841
[3] Mitch M G, Chase S J and Lannin J S 1992 *Phys. Rev. Lett.* **68** 833
[4] Zhou P, Wang K A, Eklund P C, Dresselhaus G and Dresselhaus M S 1993 *Phys. Rev.* B **48** 8412
[5] Winter J and Kuzmany H 1996 *Phys. Rev.* B **53** 655
[6] Chen X H, Taga S and Iwasa Y 1999 *Phys. Rev.* B **60** 4351
[7] van Loosdrecht P H M, van Bentum P J M and Meijer G 1992 *Phys. Rev. Lett.* **68** 1176
[8] Matus M and Kuzmany H 1993 *Appl. Phys.* A **56** 241
[9] Kelly M K and Thomsen C 1994 *Phys. Rev.* B **50** 18 572
[10] Hadjiev V G, Rafailov P M, Jantoljak H, Thomsen C and Kelly M K 1997 *Phys. Rev.* B **56** 2495
[11] Dong Z H, Zhou P, Holden J M, Eklund P C, Dresselhaus M S and Dresselhaus G 1993 *Phys. Rev.* B **48** 2862
[12] Love S P, McBranch D, Salkolka M, Coppa N V, Robinson J M, Swanson B I and Bishop A R 1994 *Chem. Phys. Lett.* **225** 170
[13] David W I F, Ibberson R M, Dennis T J S, Hare J P and Prassides K 1992 *Europhys. Lett.* **18** 219
[14] Iwasa Y, Hayashi H, Furudate T and Mitani T 1996 *Phys. Rev.* B **54** 14 960
[15] Iwasa Y, Kawaguchi M, Iwasaki H, Mitani T, Wada N and Hasegawa T 1998 *Phys. Rev.* B **57** 13 395

[16] Zhou P, Wang K A, Rao A M, Eklund O C, Dresselhaus G and Dresselhaus M S 1992 *Phys. Rev.* B **45** 10 838
[17] Fischer J E and Heiney P A 1993 *J. Phys. Chem. Solids* **54** 1725
[18] Auerbach A, Manini N and Tosatti E 1994 *Phys. Rev.* B **49** 12 998
[19] Hamanaka Y, Morimoto M, Nakashima S and Hangyo M 1995 *J. Phys.: Condens. Matter* **7** 9913
[20] Horoyski P J, Thewalt M L W and Anthony T R 1994 *Phys. Rev. Lett.* **74** 194
[21] Dolganov V K, Zharikov O V, Kremenskaja I N, Meletov K P and Ossipyan Y A 1992 *Solid State Commun.* **83** 63
[22] Fischer J E, Heiney P A, McGhie A R, Romanow W J, Denenstein A M, McCauley J P Jr and Smith A B III 1991 *Science* **252** 1288
[23] Tolbert S H, Alivisatos A P, Lorenzana H E, Kruger M B and Jeanloz R 1992 *Chem. Phys. Lett.* **188** 163
[24] Brocard F, Hricha Z, Rachdi F, Zahab A and Sauvajol J L 1994 *Solid State Commun.* **92** 281
[25] Chen X H, Takenobu T, Muro T, Fudo H and Iwasa Y 1999 *Phys. Rev.* B **60** at press